Design of magnetic spirals in layered perovskites

Extending the stability range far beyond room temperature

Shang, Tian; Canévet, Emmanuel; Morin, Mickaël; Sheptyakov, Denis; Fernández-Díaz, María Teresa; Pomjakushina, Ekaterina; Medarde, Marisa

Published in:
Science Advances

Link to article, DOI:
10.1126/sciadv.aau6386

Publication date:
2018

Document Version
Publisher's PDF, also known as Version of record

MATERIALS SCIENCE

Design of magnetic spirals in layered perovskites: Extending the stability range far beyond room temperature

Tian Shang[1,2,3]*, Emmanuel Canévet[4,5], Mickaël Morin[1,6], Denis Sheptyakov[4], María Teresa Fernández-Díaz[7], Ekaterina Pomjakushina[1], Marisa Medarde[1]*

In insulating materials with ordered magnetic spiral phases, ferroelectricity can emerge owing to the breaking of inversion symmetry. This property is of both fundamental and practical interest, particularly with a view to exploiting it in low-power electronic devices. Advances toward technological applications have been hindered, however, by the relatively low ordering temperatures T_{spiral} of most magnetic spiral phases, which rarely exceed 100 K. We have recently established that the ordering temperature of a magnetic spiral can be increased up to 310 K by the introduction of chemical disorder. Here, we explore the design space opened up by this novel mechanism by combining it with a targeted lattice control of some magnetic interactions. In Cu-Fe layered perovskites, we obtain T_{spiral} values close to 400 K, comfortably far from room temperature and almost 100 K higher than using chemical disorder alone. Moreover, we reveal a linear relationship between the spiral's wave vector and the onset temperature of the spiral phase. This linear law ends at a paramagnetic-collinear-spiral triple point, which defines the highest spiral ordering temperature that can be achieved in this class of materials. On the basis of these findings, we propose a general set of rules for designing magnetic spirals in layered perovskites using external pressure, chemical substitutions, and/or epitaxial strain, which should guide future efforts to engineer magnetic spiral phases with ordering temperatures suitable for technological applications.

INTRODUCTION

Magnetic frustration is characterized by the magnetic interactions that cannot be simultaneously satisfied (*1*–*6*) and may lead to nontrivial magnetic orders (*7*–*11*). An example of these exotic magnetically ordered phases is the spin spiral, which has received a lot of attention during the last decade because of its potential for inducing ferroelectricity in insulating materials (*12*–*16*). Stabilization of the spiral state close to room temperature (RT) is a necessary condition to use this property for magnetoelectric applications. Unfortunately, very few insulators display spiral phases above 100 K.

Besides cupric oxide (CuO) and some hexaferrites (*17*–*20*), the layered perovskite $YBaCuFeO_5$ is one of the few exceptions to this rule. However, what makes this last material truly remarkable is the extraordinary tunability of its spiral ordering temperature (T_{spiral}), which can be increased by more than 150 K by manipulating the Cu/Fe chemical disorder in the structure. We showed recently that T_{spiral} can be shifted from 154 to 310 K by adjusting the average Cu/Fe occupations n_{Cu} and n_{Fe} of the square-pyramidal sites in the crystal unit cell (Fig. 1A) (*21*). We also established the existence of a positive correlation between the spiral ordering temperature and the degree of Cu/Fe intermixing (maximal for $n_{Cu} = n_{Fe} = 50\%$). However, the most surprising observation is that tiny differences in the Cu/Fe occupations ($|n_{Cu} - n_{Fe}| \leq 6\%$) can shift T_{spiral} by more than 150 K. Such a huge positive impact of the Cu/Fe disorder in the spiral stability is remarkable and calls for further investigations aimed at both understanding and exploiting this unusual trend.

The aim of the present study is to explore the design space opened by this novel, disorder-based spiral control mechanism. After having shown its potential and limitations for the particular case of $YBaCuFeO_5$ (*21*), we combine it here with a targeted lattice tuning of some magnetic exchanges. The idea behind this is to add up the effect of both mechanisms to stabilize spin spirals at temperatures higher than those obtained using these two strategies separately. In the following, we show that, for Cu-Fe–based layered perovskites, T_{spiral} values close to 400 K can be obtained using this approach. These values are ~100 K higher than using chemical disorder alone (*21*) and expand the stability range of the spiral to a comfortable temperature region that extends well beyond RT. We also uncover the existence of an intriguing paramagnetic-collinear-spiral triple point, which defines the highest T_{spiral} value that can be achieved in this class of materials. Moreover, we find several correlations between the spiral properties and some structural parameters that can be summarized in the form of a simple set of rules for magnetic spiral design in layered perovskites. Besides overcoming limiting factors in terms of operating temperatures, these results could contribute to increase the number of materials featuring spiral phases that are stable well beyond RT and be an important step toward the technological application of magnetic spirals in spintronic devices.

The strategy followed to attain our goal is based on the particularities of the $YBaCuFeO_5$ crystal structure and the associated NN exchange couplings. A schematic representation of the layered perovskite unit cell of this material (space group *P4mm*) is shown in Fig. 1A (*22*–*24*). The A sites are occupied by equal amounts of Y^{3+} and Ba^{2+} that order in planes perpendicular to the **c** axis owing to their very different ionic radii (*25*). The B sites host Fe^{3+} and Cu^{2+} in a square-pyramidal coordination that forms slabs of "bowties" separated

[1]Laboratory for Multiscale Materials Experiments, Paul Scherrer Institut, CH-5232 Villigen PSI, Switzerland. [2]Swiss Light Source, Paul Scherrer Institut, CH-5232 Villigen PSI, Switzerland. [3]Institute of Condensed Matter Physics, École Polytechnique Fédérale de Lausanne (EPFL), CH-1015 Lausanne, Switzerland. [4]Laboratory for Neutron Scattering and Imaging, Paul Scherrer Institut, CH-5232 Villigen PSI, Switzerland. [5]Department of Physics, Technical University of Denmark, 2800 Kgs. Lyngby, Denmark. [6]Excelsus Structural Solutions (Swiss) AG PARK innovAARE, CH-5234 Villigen, Switzerland. [7]Institut Laue Langevin, 71 avenue des Martyrs, CS 20156, 38042 Grenoble CEDEX 9, France.
*Corresponding author. Email: tian.shang@psi.ch (T.S.); marisa.medarde@psi.ch (M.Me.)

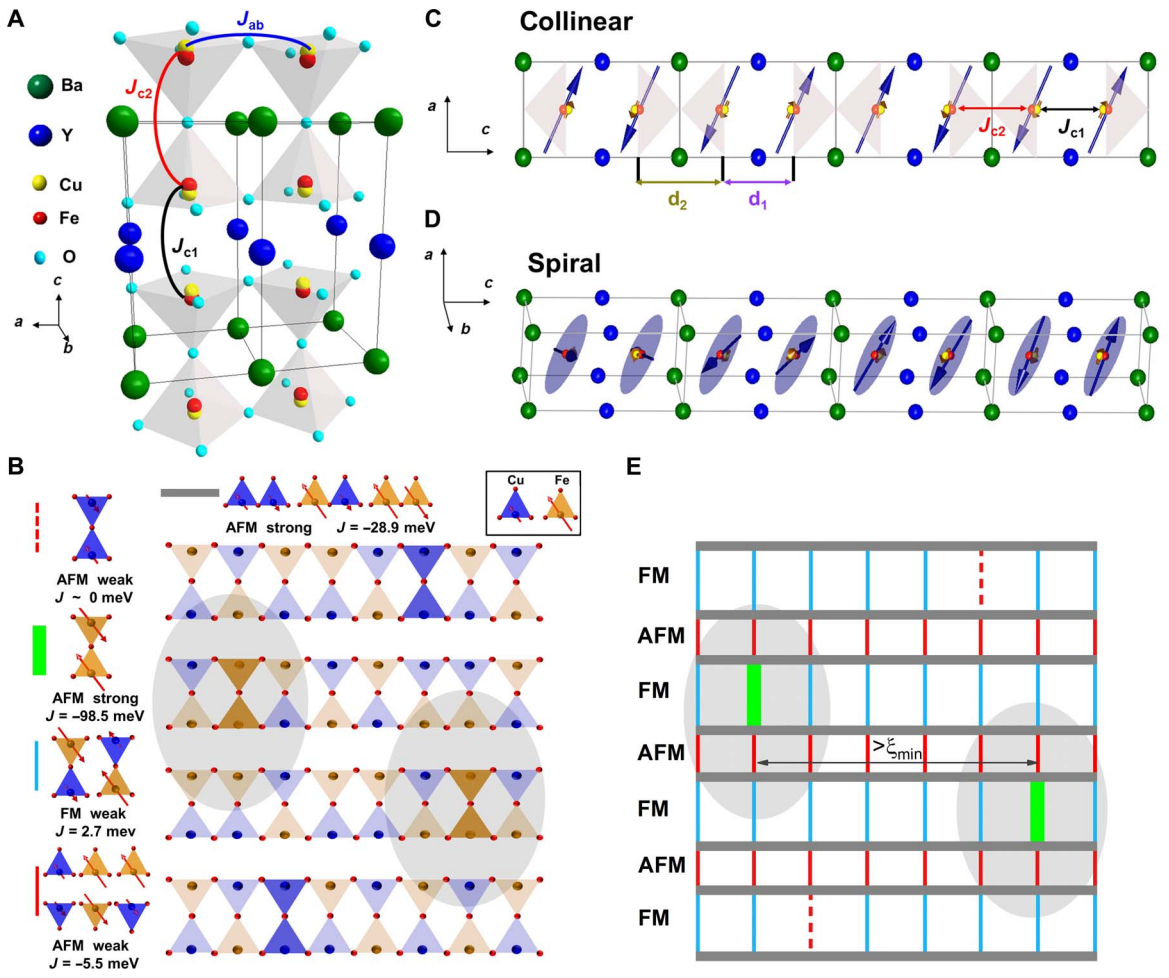

Fig. 1. Link between Cu/Fe chemical disorder and magnetic order in $YBaCuFeO_5$. (**A**) Crystal structure of $YBaCuFeO_5$ with Cu/Fe disorder in the bipyramidal sites. J_{c1} and J_{c2} denote the nearest-neighbor (NN) antiferromagnetic (AFM) and ferromagnetic (FM) couplings, respectively, along the ***c*** axis, and J_{ab} denotes the average NN AFM coupling in the **ab** plane. (**B**) Schematic representation of the correlated Cu-Fe chemical disorder in $YBaCuFeO_5$, characterized by the presence of randomly disordered Cu-Fe FM "dimers." (**C**) Magnetic structure of the commensurate collinear phase. (**D**) Magnetic structure of the incommensurate spiral phase. (**E**) The representation of (B) in terms of magnetic bonds. The impact of a few strong, randomly distributed AFM Fe-Fe "defects" is illustrated by the gray ellipses, which delimit the regions where the Cu-Fe spins lose their collinearity. Thinner bonds represent weak AFM or FM couplings, while thicker bonds indicate strong AFM couplings. The cross-talking of these regions eventually gives rise to a spiral if the in-plane separation of the Fe-Fe impurities is smaller than ξ_{min}. Note that the same number of weakly interacting Cu-Cu "defects" is necessary to preserve the material's stoichiometry. The *J* values are those of Scaramucci *et al.* (*32*).

by Y^{3+} layers. In contrast to Y and Ba, Cu and Fe display a very particular kind of correlated disorder, which is characterized by the preferential occupation of the bowties by Cu-Fe pairs (*24*). These Cu-Fe dimers are disordered in the structure (see Fig. 1B), leading to variable, preparation-dependent averaged Cu/Fe occupations of the atomic positions inside the pyramids.

The Cu-Fe dimers have very important consequences for the magnetism of $YBaCuFeO_5$. As demonstrated in (*24*, *26*), all possible in-plane NN interactions J_{ab} (Fe-Fe, Cu-Cu, and Cu-Fe) are strong and AFM (see Fig. 1, A and B). J_{c1}, one of the two NN couplings along the ***c*** axis (Fig. 1, A and C), is also AFM and disorder independent, but its value is about one order of magnitude smaller. The intra-bowtie coupling J_{c2}, comparable to J_{c1} in absolute value, is the only FM NN exchange interaction, and it is worth noting that this is only possible if the bowties are preferentially occupied by Cu-Fe pairs (i.e., if $J_{c2} = J_{Cu\text{-}Fe}$) (*24*). This set of magnetic interactions is at the origin of the collinear magnetic phase observed at high temperatures ($T < T_{collinear}$) with $\mathbf{k_c} = (^1/_2, ^1/_2, ^1/_2)$ (see Fig. 1C) (*21*, *24*, *27*–*30*). Note that despite the underlying chemical disorder, the preferential occupation of the bowties by FM Cu-Fe dimers and the nondependence of the sign of J_{ab} and J_{c1} with the Cu/Fe disorder imply that the magnetic structure can be seen as a set of ordered layers with strong in-plane AFM bonds coupled through weak, alternating FM and AFM bonds along the ***c*** axis (Fig. 1E).

At low temperatures, the k_z component of the propagation vector becomes incommensurate and the collinear magnetic order transforms into an inclined circular spiral with $\mathbf{k_i} = (^1/_2, ^1/_2, ^1/_2 \pm q)$ (Fig. 1D) (*21*, *24*, *28*, *29*, *31*). Although the ***c*** axis seems naturally more prone to a magnetic instability owing to the weakness of J_{c1} and J_{c2}, the appearance of the spiral state is surprising because these two couplings are not frustrated, and the next-NN interactions, estimated from density functional theory (DFT) calculations, either are too small or have the wrong sign to produce frustration along this direction (*24*, *26*, *32*, *33*).

RESULTS

Tuning T_{spiral} with chemical disorder

Very recently, an alternative, disorder-based mechanism has been proposed by Scaramucci and co-workers (*32*). These authors demonstrated that a magnetic spiral can be stabilized through the introduction of a few strong, randomly distributed frustrating bonds in systems featuring a single crystallographic direction with weak NN magnetic couplings. $YBaCuFeO_5$, with strong in-plane couplings and weak, alternating AFM/FM exchanges along the **c** axis (Fig. 1B), fulfills these premises (*24*, *26*). The required frustrating bonds are provided by small, preparation-dependent amounts of bowties occupied by Fe-Fe pairs (accompanied by the same amounts of Cu-Cu pairs if we assume a constant Cu/Fe ratio). Although both are energetically unfavorable (*24*), their presence at very low concentrations cannot be disregarded in real materials. Rather, the monotonic changes in the size of the bowties with increasing cooling rates suggest that their concentration could be directly linked to the degree of Cu/Fe disorder. Because of the small Cu^{2+} moment ($S = {}^1/_2$) and the extremely weak Cu-Cu coupling ($J_{Cu\text{-}Cu} \sim 0$) (dashed bonds in Fig. 1E), a Cu-Cu defect is expected to have only a minor impact in the alignment of the neighboring spins. However, an AFM Fe-Fe pair ($S = {}^5/_2$, $J_{Fe\text{-}Fe} \sim -100$ meV) (solid green bonds in Fig. 1E) constitutes an extremely strong local perturbation of the underlying collinear spin order, particularly along the ***c*** axis where the couplings are weak. This perturbation can extend to several unit cells (Fig. 1, B and E), become collective, and give rise to a spiral if (i) the Fe-Fe defects do not cluster within the **ab** plane, i.e., if they are separated by a minimal average distance ξ_{min}; (ii) the $J_{Cu\text{-}Fe}/J_{Fe\text{-}Fe}$ ratio is small enough and negative to guarantee strong local frustration; and (iii) the concentration of Fe-Fe defects n is low enough so as to avoid impurity bonds dominating the order between successive planes ($n < J_{Cu\text{-}Fe}/J_{Fe\text{-}Fe}$) (*32*, *33*).

The main prediction of this model is that both the spiral ordering temperature T_{spiral} and the magnetic modulation vector q should increase linearly with n, as long as it remains at these low levels (*32*). This is qualitatively verified in $YBaCuFeO_5$ samples prepared with different cooling rates, where the highest q and T_{spiral} values are observed for the samples quenched in liquid nitrogen (i.e., those with the largest Cu/Fe disorder and where n is expected to be the highest; see Fig. 2A) (*21*). It also suggests that the spiral ordering temperature could be further increased if a slightly larger value of n could be achieved. Since faster cooling rates are not easily achieved experimentally, we explore here an alternative strategy based on the combination of the highest possible Cu/Fe chemical disorder with a targeted lattice tuning of some magnetic exchanges.

Adding the effect of the lattice

On the basis of the previous discussion, the main candidates that influence the degree of magnetic frustration at constant Cu/Fe disorder are the NN couplings J_{c1} and J_{c2} along the ***c*** axis, which we expect to display a negative correlation with the variation of the inter-bowtie separation (d_1) and the bowtie size (d_2), respectively (Fig. 1C) (*21*). Since large changes in these two interatomic distances can be achieved through isovalent A-cation substitutions, we prepared two series of layered perovskites aimed to tune them separately. In the first one, Y^{3+} was replaced by trivalent 4*f* cations RE^{3+} with growing ionic radius (RE_{ionic}) with the purpose of acting on d_1 (RE = Lu to Dy); in the second, Ba^{2+} was partially substituted by different amounts of smaller Sr^{2+} ($0 \le x \le 0.5$) with the aim of tuning d_2. To add up the impact of both the lattice and the Cu/Fe disorder, we maximized this last parameter in all the samples, which were quenched in liquid nitrogen after the last annealing (see Materials and Methods).

The impact of this d_1 tuning on T_{spiral} is illustrated in Fig. 2B, which also shows the evolution of $T_{collinear}$ with the rare-earth ionic radius in the $REBaCuFeO_5$ series as determined from powder neutron diffraction (PND). The presence of the collinear and spiral phases in all samples was confirmed by the observation of magnetic Bragg reflections corresponding to $\mathbf{k_c} = ({}^1/_2, {}^1/_2, {}^1/_2)$ and $\mathbf{k_i} = ({}^1/_2, {}^1/_2, {}^1/_2 \pm q)$ (Fig. 2, D and E, and figs. S1 and S2). The two transition temperatures change monotonically with RE_{ionic} and display completely opposite behaviors, with $T_{collinear}$ decreasing and T_{spiral} increasing for larger ionic radii. The lowest spiral ordering temperature corresponds to $LuBaCuFeO_5$ (213 K), and the highest corresponds to $DyBaCuFeO_5$ (312 K). This last value, the only one above RT (39°C), is 2°C higher than the T_{spiral} reported in (*21*) for quenched $YBaCuFeO_5$ (Fig. 2A).

The manipulation of d_2 also has a strong impact on both transition temperatures. This is illustrated in Fig. 2C, where the evolution of $T_{collinear}$ and T_{spiral} in the $YBa_{1-x}Sr_xCuFeO_5$ family as a function of the Sr content x is shown. PND measurements again confirmed the existence of collinear and spiral phases with propagation vectors $\mathbf{k_c} = ({}^1/_2, {}^1/_2, {}^1/_2)$ and $\mathbf{k_i} = ({}^1/_2, {}^1/_2, {}^1/_2 \pm q)$ in all the materials investigated (Fig. 2, F and G, and figs. S1 and S2). We note that, contrary to the predictions of Dey *et al.* (*26*), $T_{collinear}$ decreases with x. T_{spiral} displays the opposite behavior, reaching 375 K (102°C) for $x = 0.4$. Linear extrapolation indicates that both temperatures should merge at ~395 K for $x \sim 0.49$, giving rise to a paramagnetic-collinear-spiral triple point. For $x = 0.5$, i.e., just after this point, the sample enters into a different regime characterized by an abrupt change in the stability of the spiral state. As shown in Fig. 2F and fig. S3, the magnetic reflections associated to the propagation vector $\mathbf{k_i} = ({}^1/_2, {}^1/_2, {}^1/_2 \pm q)$ are still present, but they are extremely weak. Moreover, they coexist with a new, very strong reflection corresponding to the propagation vector $\mathbf{k_{c'}} = ({}^1/_2, {}^1/_2, 0)$ and those of the $\mathbf{k_c} = ({}^1/_2, {}^1/_2, {}^1/_2)$ collinear phase. These observations suggest that the spiral state is abruptly suppressed and replaced by a new AFM phase beyond the crossing of the $T_{collinear}$ and T_{spiral} lines.

The temperature dependence of q for the $REBaCuFeO_5$ and $YBa_{1-x}Sr_xCuFeO_5$ series and that of $YBaCuFeO_5$ prepared using different cooling rates (*21*) are shown in Fig. 3 (A to C). For the samples with the lowest T_{spiral}, we observe a smooth, continuous decrease of q characteristic of second-order phase transitions. This behavior is progressively replaced by an abrupt collapse of q in the samples with higher T_{spiral}, suggesting that the collinear-to-spiral transition changes from second to first order by approaching the $T_{spiral} = T_{collinear}$ point (fig. S3). The evolution of the spiral plane inclination (φ_G) and the q value (q_G) at 10 K is shown in Fig. 3 (D to F). For the three series of samples, we observe a clear, positive correlation among T_{spiral}, φ_G, and q_G. In each family, the highest T_{spiral} is observed for the sample with the largest φ_G, which reaches values close to 90° for RE = Dy. This corresponds to a perfect cycloid, indicating that the samples with the highest spiral ordering temperature have the potential of displaying the largest saturation polarization (*15*, *16*). Establishing whether this is the case is beyond the scope of this study and will require further experimental and theoretical work.

An interesting observation, common to all the samples investigated in this study, is the existence of a linear relationship between the ordering temperature and the ground-state periodicity of the spiral. This can be better appreciated in Fig. 4, where the evolution of T_{spiral} with q_G for the three series of samples is shown. We note that

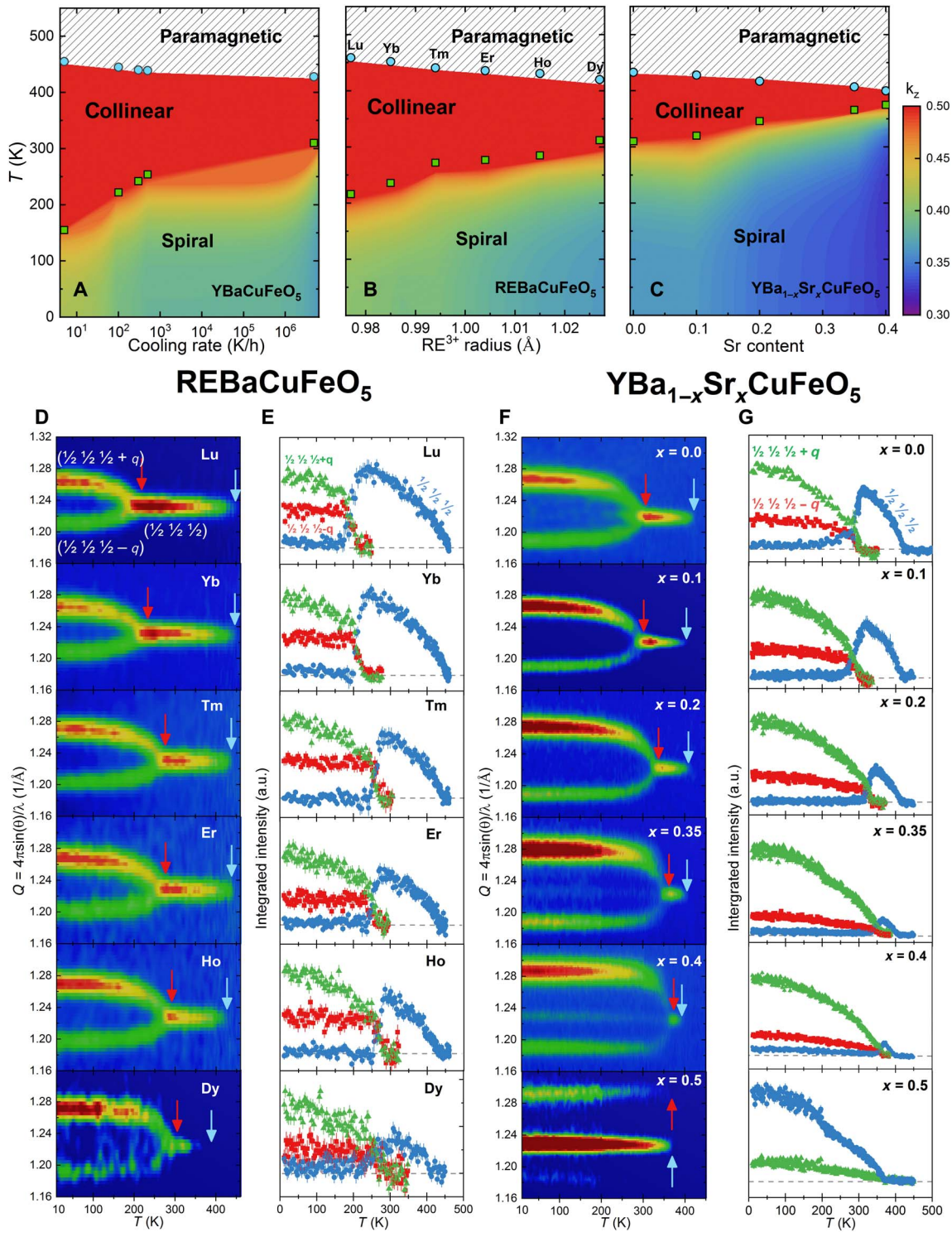

Fig. 2. Stability of the collinear and spiral phases with different tuning parameters. (**A** to **C**) Evolution of $T_{collinear}$ and T_{spiral} using different tuning parameters: (A) $YBaCuFeO_5$ prepared with different cooling rates [adapted from (*21*)]. (B) Replacement of Y^{3+} by a rare-earth cation (RE^{3+}). (C) Replacement of Ba^{2+} by Sr^{2+}. The $T_{collinear}$ and T_{spiral} values are those determined from PND. The background color represents the *z* component of the magnetic propagation vector (k_z), which changes from $^1/_2$ in the collinear phase to $^1/_2 \pm q$ in the spiral phase (only the $^1/_2 - q$ incommensurate satellite is used in the figures). (**D** to **G**) Signatures of the collinear and spiral phases in the PND patterns. The contour maps show the temperature dependence of the positions and the intensities of the commensurate ($^1/_2$, $^1/_2$, $^1/_2$) magnetic Bragg reflection and the incommensurate ($^1/_2$, $^1/_2$, $^1/_2 \pm q$) satellites for the $REBaCuFeO_5$ (D) and $YBa_{1-x}Sr_xCuFeO_5$ (F) series. The blue and red arrows indicate the ordering temperatures $T_{collinear}$ and T_{spiral}, respectively. The integrated intensities are shown in (E) for $REBaCuFeO_5$ and in (G) for $YBa_{1-x}Sr_xCuFeO_5$. For the Sr-doped sample with $x = 0.5$, the "minus" incommensurate satellite ($^1/_2$, $^1/_2$, $^1/_2 - q$) was extremely weak (see also fig. S3). Hence, only the integrated intensity of the "plus" satellite ($^1/_2$, $^1/_2$, $^1/_2 + q$) is shown. The error bars of the integrated intensities are the SDs obtained from three Gaussian least-squares fits of the ($^1/_2$, $^1/_2$, $^1/_2$) Bragg reflection and its incommensurate satellites carried out using the Igor software. a.u., arbitrary units.

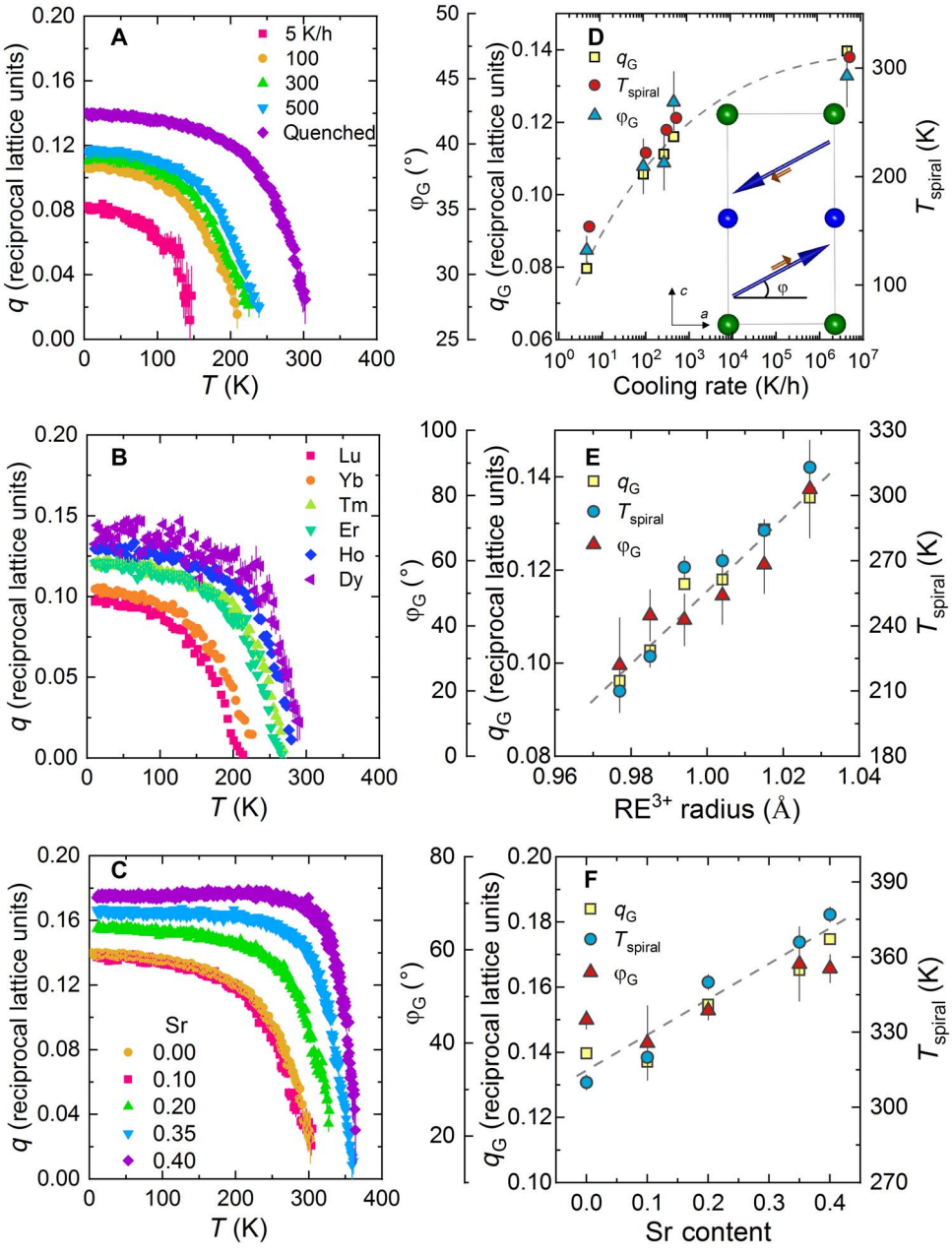

Fig. 3. Evolution of magnetic spiral properties with different tuning parameters. (**A** to **C**) Temperature dependence of the magnetic modulation vector q in $YBaCuFeO_5$ using different tuning parameters: (A) Cooling rate [adapted from (*21*)]. (B) Replacement of Y^{3+} by a rare-earth cation (RE^{3+}). (C) Replacement of Ba^{2+} by Sr^{2+}. (**D** to **F**) Evolution of T_{spiral}, the ground-state values (10 K) of the magnetic modulation vector (q_G), and the inclination of the spiral rotation plane (φ_G) using different tuning parameters: (D) Cooling rate [adapted from (*21*)]. (E) Replacement of Y^{3+} by a rare-earth cation (RE^{3+}). (F) Replacement of Ba^{2+} by Sr^{2+}. The inset in (D) shows the definition of the inclination angle φ_G. The dashed lines are guides to the eye and indicate the positive correlation among T_{spiral}, q_G, and φ_G. The values for $REBaCuFeO_5$ and $YBa_{1-x}Sr_xCuFeO_5$ families were extracted from Rietveld fits of the DMC data recorded at 10 K (fig. S5). The error bars of q_G and φ_G, listed in tables S2 and S3, are the SDs obtained from the fits of the magnetic structure using the FullProf Suite Rietveld package (*50*).

the extrapolation of the linear law toward low T_{spiral} values crosses the origin (i.e., $T_{collinear} = 0$ for $q_G = 0$), whereas in the high q_G side, $T_{collinear}$ and T_{spiral} converge to a common value of ~395 K for q_G ~ 0.18. The sudden disappearance of the spiral and the observation of a new magnetic phase close to this point suggest the existence of a limiting value for both the spiral's periodicity and ordering temperature. In other words, 395 K is most probably the highest T_{spiral} value that can be reached in Cu-Fe–based layered perovskites. To the best of our knowledge, it is the highest spiral ordering temperature reported for a transition metal oxide, the only comparable example being the Néel temperature of the transverse conical spiral phase in the hexaferrite $Sr_3Co_2Fe_{24}O_{41}$ [~400 K; see (*19*)]. Moreover, it is comfortably far from RT, an important point regarding applications, and almost 100 K higher than the highest T_{spiral} value previously reported for $YBaCuFeO_5$ using chemical disorder alone (310 K).

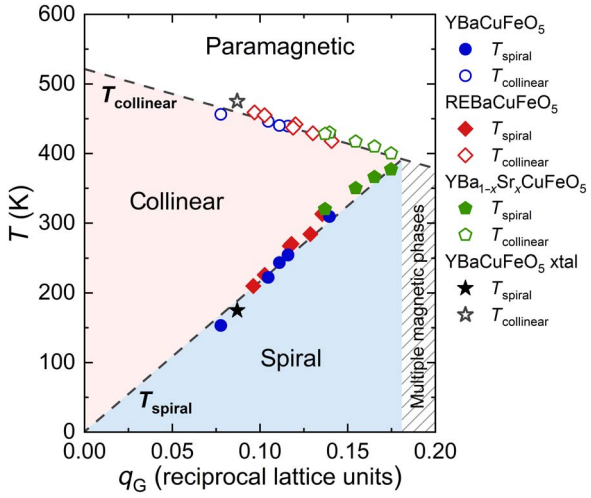

Fig. 4. Linear relationship between T_{spiral} and q_G in AA'CuFeO$_5$ layered perovskites. Correlation between T_{spiral} and the ground-state magnetic modulation vector q_G in three families of AA'CuFeO$_5$ layered perovskites: YBaCuFeO$_5$ prepared with different cooling rates [full blue symbols; data from (*21*)], REBaCuFeO$_5$ with RE = Lu to Dy (full red symbols), and YBa$_{1-x}$Sr$_x$CuFeO$_5$ with $0 \le x \le 0.4$ (full green symbols). The full black star corresponds to the (q_G, T_{spiral}) point reported for a YBaCuFeO$_5$ single crystal in (*29*). The $T_{collinear}$ values of all samples (open symbols) are also shown to illustrate its convergence with T_{spiral} at $q_G \sim 0.18$. The T_{spiral} and $T_{collinear}$ values are those determined from PND (tables S1). The error bars of q_G, listed in tables S2 and S3, are the SDs obtained from the fits of the magnetic structure using the FullProf Suite Rietveld package (*50*), and they are smaller than the marker's size.

Chemical disorder versus lattice tuning

After demonstrating the success of our combined approach, we investigate in detail the associated changes in the crystal structure with the aim of obtaining additional insight into their link with the degree of magnetic frustration. We use high-resolution PND (fig. S6) to obtain precise values of the different structural parameters for the REBaCuFeO$_5$ and YBa$_{1-x}$Sr$_x$CuFeO$_5$ series, which we compare with those obtained for YBaCuFeO$_5$ prepared using different cooling rates (*21*). We first check the average Cu/Fe occupancies n_{Cu} and n_{Fe} of the bipyramidal sites, which we expected to be very similar owing to the quenching procedure used during the synthesis. The obtained values, shown in Fig. 5 (A to C) and tables S2 and S3, confirm a high degree of disorder in all the samples, which display average Cu/Fe occupancies very close to 50%.

The evolution of the lattice parameters and the tetragonal distortion $c/2a$ for the three series are summarized in Fig. 5 (D to L). On the basis of the results obtained for YBaCuFeO$_5$ with different degrees of Cu/Fe disorder, we established in (*21*) an empirical, positive correlation between $c/2a$ and T_{spiral} and suggested the use of this parameter for T_{spiral} control purposes. Although a similar correlation was observed for the REBaCuFeO$_5$ series (Fig. 5K), Fig. 5L reveals the opposite behavior in the Sr-substituted family. This suggests that the use of $c/2a$ for the control of magnetic frustration, of potential interest in thin film growth, cannot be generalized to all Cu/Fe layered perovskites.

We investigate now the presence of correlations between T_{spiral} and the different NN interatomic distances and angles. In fig. S4, we have represented the evolution of the average in-plane Cu/Fe-O distance and the average superexchange angle for the three families. As for the lattice parameters, T_{spiral} does not display a monotonic behavior with any of those parameters. We thus conclude that the in-plane distances and angles are not suitable parameters for controlling the spiral ordering temperature. The modification of the inter- and intra-bowtie distances d_1 and d_2 along the ***c*** axis and their ratio d_1/d_2 for the three series are summarized in Fig. 5 (M to U). The longest d_1 and shortest d_2 values are systematically observed in the three families for the samples with the highest T_{spiral} and lowest $T_{collinear}$ values. Moreover, the d_1/d_2 ratio displays a positive correlation with the spiral ordering temperature in the three series. This common behavior indicates that, contrary to $c/2a$, the d_1/d_2 ratio is a good parameter for the control of magnetic frustration in Cu/Fe-based layered perovskites.

Despite a common positive correlation between T_{spiral} and d_1/d_2 ratio, Fig. 5 unravels the existence of large differences among the structural modifications in the three series. The smallest changes in the lattice parameters and the interatomic distances correspond to the YBaCuFeO$_5$ samples with different degrees of Cu/Fe disorder. These tiny variations give rise to changes in T_{spiral} of more than 150 K, much larger than those in the REBaCuFeO$_5$ (~100 K) and YBa$_{1-x}$Sr$_x$CuFeO$_5$ (~90 K) series, where the variation of the lattice parameters and interatomic distances is much more pronounced. This is better appreciated in Fig. 5V, where the evolution of T_{spiral} with d_1/d_2 is displayed. This parameter, which reflects the relative strength J_{c2}/J_{c1} of the couplings along the ***c*** axis, changes very little in the YBaCuFeO$_5$ samples with different degrees of disorder (0.41%). However, it increases by more than 1.7% between the two extremes of the YBa$_{1-x}$Sr$_x$CuFeO$_5$ family and by 4.6% in the REBaCuFeO$_5$ series. These results confirm the exceptional efficiency of chemical disorder alone for T_{spiral} tuning. On the other side, our data also show that a comparable efficiency in terms of T_{spiral} increase can be reached at a fixed degree of chemical disorder by acting exclusively on the lattice. A particularly interesting observation is that the impact of both mechanisms on the spiral ordering temperature is additive: Once the highest T_{spiral} value is reached by manipulating the Cu/Fe disorder, it can be further increased through the maximization of the d_1/d_2 ratio. This allows T_{spiral} tuning over unprecedentedly large temperature ranges, providing, at the same time, a versatile tool for stabilizing spin spirals at temperatures well beyond RT.

Experiment versus theory

Having presented the experimental facts, we now compare our observations with the predictions of the random frustrating bonds (RFB) model proposed by Scaramucci and co-workers (*32*, *33*). The main prediction of this model is that both T_{spiral} and q should increase with the concentration of Fe-Fe frustrating bonds n. Since n is in turn correlated with the degree of average Cu/Fe disorder, this prediction explains well the behavior reported for the YBaCuFeO$_5$ samples prepared with different cooling rates (*21*). However, it is difficult to conciliate the huge T_{spiral} changes observed in the YBa$_{1-x}$Sr$_x$CuFeO$_5$ and REBaCuFeO$_5$ families, where the Cu/Fe disorder was kept approximately constant. A similar situation is observed with a second prediction, namely, the existence of a proportionality law between T_{spiral} and q_G. This linear law should be verified by samples with different degrees of disorder, and this is indeed the case for the YBaCuFeO$_5$ series prepared with different cooling rates (full blue circles in Fig. 4) (*21*). More intriguing is the fact that the very same law is also verified by the YBa$_{1-x}$Sr$_x$CuFeO$_5$ (full green pentagons) and REBaCuFeO$_5$ families (full red diamonds) and even by the YBaCuFeO$_5$ single crystal from (*29*) (black star) to a very good approximation. This unexpected observation cannot be explained within the framework of the RFB model and calls for the explicit consideration of lattice's impact in the different magnetic exchanges.

A third point needing further theoretical work is the origin of the intersection of T_{spiral} and $T_{collinear}$ for $q_G \sim 0.18$ and the sudden

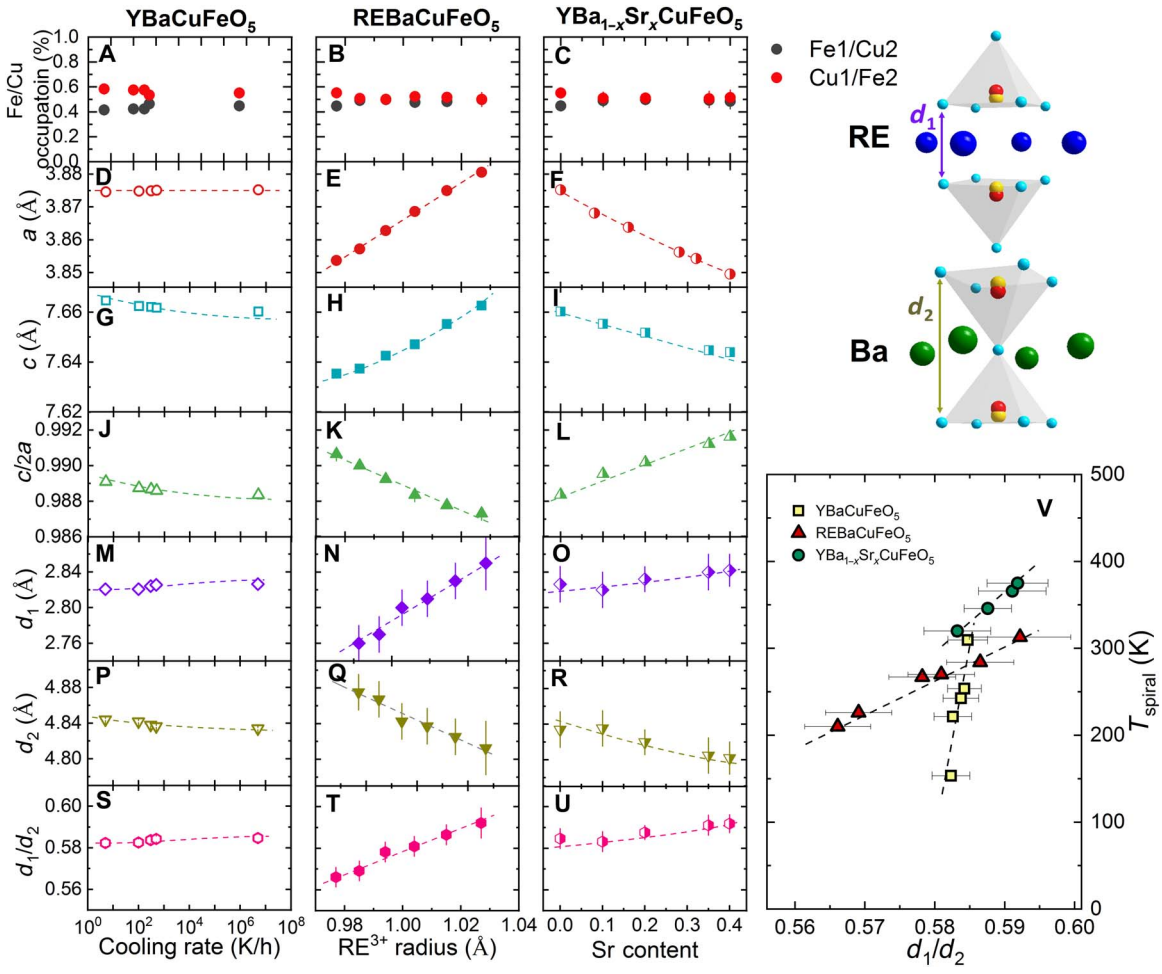

Fig. 5. Link between crystal structure and magnetic ordering temperatures. (**A** to **U**) Evolution of selected structural parameters as a function of the cooling rate [$YBaCuFeO_5$; data from (*21*)], the rare-earth ionic radius ($REBaCuFeO_5$), and the Sr content x ($YBa_{1-x}Sr_xCuFeO_5$). (A to C) Average Cu/Fe occupation in the pyramids. (D to I) Lattice parameters **a** and **c**. (J to L) Tetragonal distortion $c/2a$. (M to O) Distance d_1 between the bipyramidal layers along the **c** axis. (P to R) Thickness d_2 of the bipyramidal layers. (S to U) d_1/d_2 ratio. (**V**) Evolution of T_{spiral} with d_1/d_2 ratio. The yellow, red, and green colors correspond to $YBaCuFeO_5$ prepared with different cooling rates, $REBaCuFeO_5$ (RE = Lu to Dy), and $YBa_{1-x}Sr_xCuFeO_5$ (x = 0 to 0.4), respectively. The T_{spiral} and $T_{collinear}$ values are those determined from PND (tables S1). The dashed lines are guides to the eye. All structural parameters were extracted from the Rietveld fits of the high-resolution PND data at RT (tables S2 and S3). The error bars are the SDs provided by the FullProf Suite Rietveld package (*50*).

replacement of the spiral state by a second commensurate AFM phase beyond this point. Given that it coincides with the smallest d_2 (i.e., largest J_{c2}) values of our study, the disappearance of the spiral could be tentatively ascribed to the point where the AFM couplings between Fe-Fe impurities become so large that the FM coupling of the bipyramids occupied by Cu-Fe pairs can no longer compete and the magnetic frustration is suppressed. The result would be a magnetic structure where all NN couplings are AFM, in agreement with the observation of the new magnetic propagation vector $\mathbf{k}_{c'} = (^1/_2, ^1/_2, 0)$. However, it is not clear why this point should coincide with the intersection of the $T_{collinear}$ and T_{spiral} lines. Another intriguing observation is the continuous evolution of the spiral-to-collinear phase transition from second to first ordering by approaching the paramagnetic-collinear-spiral triple point. Information about the behavior of the different magnetic phases beyond the crossing of the $T_{collinear}$ and T_{spiral} lines should help to understand its exact nature and, in particular, to clarify whether we could be in the presence of a Lifschitz point (*34*, *35*). We also note that its increased entropy at the crossing makes this point potentially interesting for the search of exotic magnetic states in the presence of external perturbations such as magnetic fields or elevated pressures (*34*, *36*, *37*).

Toward spiral design in layered perovskites

An important outcome of the structural property correlations presented in previous sections is that they enable the proposal of a simple set of rules for the design of high-temperature magnetic spirals in other $AA'BB'O_5$ layered perovskites with B-site disorder. Besides maintaining electric neutrality, the most critical point is to identify B/B′ cation pairs of comparable sizes and affinity for square-pyramidal coordination. They should be also capable of producing weak, alternating FM and AFM couplings along the **c** axis, and large in-plane exchange constants, with a very large value for one of the two J_{BB} or $JJ_{BB'}$ couplings. The choice is mostly limited by the relatively small number of pairs resulting in FM coupling within the pyramids, but among 3*d* transition metals, Cu^{2+}/Cu^{3+}, Cu^{2+}/Co^{3+}(high spin), Cu^{2+}/Mn^{3+}, or Mn^{2+}/Co^{3+}(low spin) could be possible candidates if J_{BB} and $J_{B'B'}$ have the appropriate

absolute values. Ab initio DFT estimations of the magnetic exchanges, particularly for 4*d* and 5*d* pairs, will be highly desirable and shall increase the number of potential candidates. The choice of the A/A′ cations requires ionic radii different enough to stabilize the layered perovskite structure. However, the highest T_{spiral} values can be achieved when the ionic radius of the A cation close to the apical oxygen is small and the $r^{A}_{ionic} - r^{A'}_{ionic}$ difference is as small as possible (Fig. 5). Concerning thin-film design, we saw that $c/2a$ alone is not a good parameter for T_{spiral} control. Hence, high T_{spiral} values can be a priori stabilized under both tensile and compressive strain as long as the rules concerning the choice of the A and B cations are fulfilled.

We can also speculate on the expected behavior of T_{spiral} under external pressure. According to our findings, this will depend on the behavior of d_1/d_2, i.e., on the relative compressibility of these two distances. In general, bonds involving cations with high coordination or low valence expand or compress faster than those with cations in low coordination or with high valence (*38*, *39*). d_2, involving 12 (Ba^{2+}–O^{2-}) bonds, is thus expected to compress faster than d_1, where only 8 (RE^{3+}–O^{2-}) bonds contribute. Since this will result in a smaller d_1/d_2 ratio, a decrease of T_{spiral} is thus predicted under the application of external pressure.

To summarize, we have experimentally validated an emerging route for stabilizing spin spirals up to temperatures far beyond RT. Our approach, based on the combination of chemical disorder with a targeted lattice tuning of some magnetic exchanges, takes full advantage of the additivity of these two mechanisms. As a result, the stability domain of the spiral magnetic order can be tuned over unprecedentedly large temperature ranges. In the particular case of Cu/Fe-based layered perovskites, we demonstrate that T_{spiral} values close to 400 K can be reached using this strategy. This value is ~100 K higher than using chemical disorder alone (*21*) and comfortably far beyond RT. We also reveal the existence of a linear relationship between the spiral's ordering temperature and periodicity, a paramagnetic-collinear-spiral triple point, as well as several correlations between the spiral properties and some structural parameters. We discuss these results in light of a recently proposed RFB-based mechanism and propose a simple set of rules for the design of magnetic spirals in isostructural layered perovskites by using external pressure, chemical substitutions, or epitaxial strain. Besides overcoming one of the main hindrances for applications, these results could accelerate the discovery of other materials featuring spiral phases stable well beyond RT, paving the way toward the long-sought technological use of magnetic spirals in spintronic devices.

MATERIALS AND METHODS

Materials synthesis

The $REBaCuFeO_5$ and $YBa_{1-x}Sr_xCuFeO_5$ polycrystalline samples were prepared using the solid-state reaction method. High-purity RE_2O_3 or Y_2O_3 (99.995 to 99.998%; Aldrich/Alfa Aesar), $SrCO_3$ (99.995%; Aldrich), $BaCO_3$ (99.997%; Alfa Aesar), CuO (99.995%; Alfa Aesar), and Fe_2O_3 (99.998%; Alfa Aesar) powders were used as starting materials. Dehydrated rare-earth oxide powders were obtained by heating them at 1223 K for 15 hours. The required stoichiometric amounts of RE_2O_3, $SrCO_3$, $BaCO_3$, CuO, and Fe_2O_3 were then weighted, thoroughly grounded, and heated at a rate of 300 K/h up to the synthesis temperature T_s (= 1323 to 1430 K), which was optimized for every sample using thermogravimetric analysis under He/O_2 gas flow. The powders were then annealed for 50 hours at this temperature under oxygen gas flow. The obtained materials were cooled in the furnace down to RT, thoroughly grounded again, pressed into pellets, and sintered at T_s for another 50 hours. After this treatment, all samples were quenched into liquid nitrogen. Small pieces were kept solid for their use in magnetization measurements, and the rest were pulverized and subsequently used in PND experiments. The phase purity of all samples was checked using laboratory powder x-ray diffraction at RT using a Bruker D8 Advance diffractometer with Cu K_α radiation. All samples were very well crystallized and free of impurities within the limit of this technique (~1%).

Magnetic susceptibility

DC magnetization (M) measurements were performed in a superconducting quantum interference device magnetometer (MPMS-XL 7T, Quantum Design). Small pellets (diameter ~ 3 mm, height ~ 1 mm, mass ~ 15 to 25 mg) from the same batches as the samples used for the PND measurements were measured between 2 and 400 K by heating under a magnetic field of $\mu_0 H = 0.5$ T after being cooled down to 2 K in zero field. The magnetization was further measured between 300 and 600 K using a high-temperature insert. The samples, mounted on transparent drinking straws for the measurements below 400 K, were dismounted and wrapped in aluminum foil as described in (*40*) for the measurements above this temperature. The signal from the aluminum foil, measured separately, was found to be temperature independent and negligible when compared with the sample's magnetization. For the samples with magnetic RE^{3+} cations, the magnetic transitions from the Cu/Fe sublattice are difficult to observe in the magnetization data because of the large paramagnetic contribution of the RE^{3+} moments, and they have been missed in some previous studies (*41*). However, they can still be tracked in the first derivatives of the DC inverse susceptibility $1/\chi^{DC} = H/M$ (fig. S1). The values of $T_{collinear}$ and T_{spiral} derived from this technique correspond to the midpoint of the step-like anomalies in the $1/\chi^{DC}$ derivative, which coincides with the χ^{DC} maximum in the $YBa_{1-x}Sr_xCuFeO_5$ series.

Although the $REBaCuFeO_5$ samples were also synthesized in the past (*42*, *43*), the existence of magnetic transitions has only been reported for a few of them (*41*, *44*–*47*), and there is no apparent systematics between the reported ordering temperatures and the RE ionic radii. A similar situation was observed in the $YBa_{1-x}Sr_xCuFeO_5$ series, where the presence of spiral phases was either disproven (*48*) or not demonstrated (*49*) in previous studies. As shown in Fig. 2C, this is not the case in this study, where the collinear and spiral phases are observed for all samples. Moreover, $T_{collinear}$ and T_{spiral} change in a monotonic way as a function of both the RE ionic radius and the Sr content *x*.

Differential scanning calorimetry

The paramagnetic-to-collinear phase transition at $T_{collinear}$ was also measured by differential scanning calorimetry (DSC) for $REBaCuFeO_5$ and $YBa_{1-x}Sr_xCuFeO_5$ powder samples by using a NETZSCH DSC 204F1 device. Fine powders (mass, ~30 mg) were sealed into aluminum crucibles and heated up to 670 K with a rate of 15 K/min under Ar gas flow. The data were acquired during the heating process (see fig. S2).

Powder neutron diffraction

PND measurements were carried out at the Swiss Spallation Neutron Source (SINQ) of the Paul Scherrer Institute in Villigen, Switzerland, and the Institut Laue-Langevin (ILL) in Grenoble, France. The $REBaCuFeO_5$ and $YBa_{1-x}Sr_xCuFeO_5$ powder samples were introduced in cylindrical vanadium cans (diameter = 6 mm, height = 5 cm) and mounted on the stick of a helium cryostat (2 to 300 K) and a cryofurnace

(2 to 500 K). PND patterns were continuously recorded at the powder diffractometer DMC (cold neutron powder diffractometer) [pyrolitic graphite (002): λ = 2.458 Å, λ = 4.507 Å, and $2\theta_{step}$ = 0.1°] while ramping the temperature from 10 to 480 K. Longer acquisitions for magnetic structure refinements were made at 10 K. High-resolution patterns at both 10 and 300 K were also recorded at the powder diffractometer HRPT (high-resolution powder diffractometer for thermal neutrons) [Ge (822): $2\theta_{step}$ = 0.05° and λ = 1.154 Å] and D2B (high-resolution two-axis diffractometer) [Ge (335): $2\theta_{step}$ = 0.05° and λ = 1.594 Å]. The wavelengths and zero offsets were determined using a NAC ($Na_2Al_{12}Ca_3F_{14}$) reference powder sample. In the case of $DyBaCuFeO_5$, the impact of the relatively large neutron absorption cross section of natural dysprosium [994(13) barn] in the data was corrected by including in the refinements the μR values determined experimentally for the different wavelengths. The background from the sample environment was minimized through 5′ collimators (D2B) and an oscillating radial collimator (HRPT). The values of $T_{collinear}$ and T_{spiral} derived from this technique correspond, respectively, to the setup and the maximum of the magnetic Bragg reflection ($^1/_2$, $^1/_2$, $^1/_2$) that roughly coincide with the values determined from χ^{DC} and DSC (see figs. S1 and S2 and tables S1).

Data analysis

All diffraction data were analyzed using the Rietveld package FullProf Suite (*50*). The structural refinements for the $REBaCuFeO_5$ series were carried out by combining both HRPT and D2B datasets recorded at RT and 10 K. For $YBa_{1-x}Sr_xCuFeO_5$ samples, HRPT data recorded at RT and 10 K were used for the fits of the crystal structure (fig. S6). The magnetic refinements were performed on DMC data recorded at 10 K by fixing the structural parameters as determined from the refinements of the HRPT and D2B patterns (fig. S5). We used the noncentrosymmetric space group *P4mm* for the description of the crystal structure. The choice was motivated by the fact that, contrary to the centrosymmetric space group *P4/mmm*, *P4mm* enables the refinement of the occupation of the split Cu and Fe sites.

The Cu/Fe disorder was described by splitting the atomic position ($^1/_2$, $^1/_2$, *z*) inside the two pyramidal sites of the unit cell, as shown in tables S2 and S3. In the fully disordered case, both positions are equally occupied in all pyramids (i.e., $n_{Fe} = n_{Cu}$ = 50%), whereas full Cu/Fe order corresponds to n_{Cu} = 100% and n_{Fe} = 0 (or n_{Cu} = 0 and n_{Fe} = 100%). As shown in tables S2 and S3, the samples investigated in this work are very close to the first scenario, i.e., of $|n_{Cu} - n_{Fe}|$ very close to zero. Note that Rietveld fits are not sensible to occupational correlations. The Cu/Fe disorder is thus assumed to be random, and the refined n_{Cu} and n_{Fe} values represent the average values over the full sample.

Anisotropic Debye-Waller factors were used for all atoms with the exception of Y/RE (nearly isotropic) [see (*21*)], Cu, and Fe. The *z* coordinates of the two basal oxygen sites O2 and O2′ were refined separately, but their mean-square displacements were restricted to have the same value (tables S2 and S3). No signature of interstitial oxygen at the ($^1/_2$, $^1/_2$, *z*) atomic position could be observed, indicating that deviations from the sample's formula stoichiometry, if any, were within the detection limit of PND in all the samples investigated. For the $YBa_{1-x}Sr_xCuFeO_5$ sample with x = 0.5, we could not find any evidence of alternating Ba/Sr layers, recently predicted for $x \geq 0.5$ (*26*) and easy to identify because of the associated doubling of the **c** lattice parameter.

The collinear and spiral magnetic structures were described according to the models reported in (*18*). The best fits obtained at 10 K for all samples are shown in fig. S5. The ratio between the $Fe^{3+}(3d^5$ HS) and $Cu^{2+}(3d^9)$ magnetic moments was restricted to be the same as their free-ion, spin-only values (5:1). In the temperature regions where the collinear and spiral phases coexist, the Fe and Cu magnetic moments were restricted to have the same value and the same inclination with respect to the **ab** plane in the two magnetic phases.

SUPPLEMENTARY MATERIALS

Supplementary material for this article is available at http://advances.sciencemag.org/cgi/content/full/4/10/eaau6386/DC1

Fig. S1. Magnetic susceptibility.
Fig. S2. Differential scanning calorimetry.
Fig. S3. Magnetic phase coexistence and percentage of collinear and spiral phases.
Fig. S4. Evolution of the in-plane interatomic distances and angles.
Fig. S5. Rietveld fits at 10 K.
Fig. S6. Rietveld fits at RT.
Table S1. Spiral (T_{spiral}) and collinear ($T_{collinear}$) magnetic transition temperatures for the $REBaCuFeO_5$ (RE = Lu to Dy) and $YBa_{1-x}Sr_xCuFeO_5$ (x = 0 to 0.4) series.
Table S2. Results of the Rietveld fits of the PND patterns for the $REBaCuFeO_5$ (RE = Lu to Dy) family at RT and 10 K.
Table S3. Results of the Rietveld fits of the PND patterns for $YBa_{1-x}Sr_xCuFeO_5$ (x = 0 to 0.5) family at RT and 10 K.

REFERENCES AND NOTES

1. S. T. Bramwell, M. J. P. Gingras, Spin ice state in frustrated magnetic pyrochlore materials. *Science* **294**, 1495–1501 (2001).
2. S. Gao, O. Zaharko, V. Tsurkan, Y. Su, J. S. White, G. S. Tucker, B. Roessli, F. Bourdarot, R. Sibille, D. Chernyshov, T. Fennell, A. Loidl, Ch. Rüegg, Spiral spin-liquid and the emergence of a vortex-like state in $MnSc_2S_4$. *Nat. Phys.* **13**, 157–161 (2017).
3. L. Balents, Spin liquids in frustrated magnets. *Nature* **464**, 199–208 (2010).
4. T. Fennell, P. P. Deen, A. R. Wildes, K. Schmalzl, D. Prabhakaran, A. T. Boothroyd, R. J. Aldus, D. F. McMorrow, S. T. Bramwell, Magnetic coulomb phase in the spin ice $Ho_2Ti_2O_7$. *Science* **326**, 415–417 (2009).
5. R. Sibille, E. Lhotel, M. C. Hatnean, G. J. Nilsen, G. Ehlers, A. Cervellino, E. Ressouche, M. Frontzek, O. Zaharko, V. Pomjakushin, U. Stuhr, H. C. Walker, D. T. Adroja, H. Luetkens, C. Baines, A. Amato, G. Balakrishnan, T. Fennell, M. Kenzelmann, Coulomb spin liquid in anion-disordered pyrochlore $Tb_2Hf_2O_7$. *Nat. Commun.* **8**, 892 (2017).
6. E. S. Dreier, S. L. Holm, K. Lønbæk, U. B. Hansen, M. Medarde, I. Živković, P. Babkevich, M. Ruminy, N. Casati, A. Piovano, S. Rols, G. J. Nilsen, M. Boehm, M. Skoulatos, J. Schefer, H. M. Rønnow, T. Fennell, K. Lefmann, 24-spin clusters in the mineral boleite $KPb_{26}Ag_9Cu_{24}Cl_{62}(OH)_{48}$. *Phys. Rev. B* **97**, 014416 (2018).
7. S. Mühlbauer, B. Binz, F. Jonietz, C. Pfleiderer, A. Rosch, A. Neubauer, R. Georgii, P. Böni, Skyrmion lattice in a chiral magnet. *Science* **323**, 915–919 (2009).
8. B. Thielemann, Ch. Rüegg, H. M. Rønnow, A. M. Läuchli, J.-S. Caux, B. Normand, D. Biner, K. W. Krämer, H.-U. Güdel, J. Stahn, K. Habicht, K. Kiefer, M. Boehm, D. F. McMorrow, J. Mesot, Direct observation of magnon fractionalization in the quantum spin ladder. *Phys. Rev. Lett.* **102**, 107204 (2009).
9. J. S. White, T. Honda, K. Kimura, T. Kimura, Ch. Niedermayer, O. Zaharko, A. Poole, B. Roessli, M. Kenzelmann, Coupling of magnetic and ferroelectric hysteresis by a multicomponent magnetic structure in Mn_2GeO_4. *Phys. Rev. Lett.* **108**, 077204 (2012).
10. L. C. Chapon, G. R. Blake, M. J. Gutmann, S. Park, N. Hur, P. G. Radaelli, S.-W. Cheong, Structural anomalies and multiferroic behavior in magnetically frustrated $TbMn_2O_5$. *Phys. Rev. Lett.* **93**, 177402 (2004).
11. N. J. Perks, R. D. Johnson, C. Martin, L. C. Chapon, P. G. Radaelli, Magneto-orbital helices as a route to coupling magnetism and ferroelectricity in multiferroic $CaMn_7O_{12}$. *Nat. Commun.* **3**, 1277 (2012).
12. T. Kimura, T. Goto, H. Shintani, K. Ishizaka, T. Arima, Y. Tokura, Magnetic control of ferroelectric polarization. *Nature* **426**, 55–58 (2003).
13. N. A. Spaldin, M. Fiebig, The renaissance of magnetoelectric multiferroics. *Science* **309**, 391–392 (2005).
14. M. Kenzelmann, A. B. Harris, S. Jonas, C. Broholm, J. Schefer, S. B. Kim, C. L. Zhang, S.-W. Cheong, O. P. Vajk, J. W. Lynn, Magnetic inversion symmetry breaking and ferroelectricity in $TbMnO_3$. *Phys. Rev. Lett.* **95**, 087206 (2005).
15. H. Katsura, N. Nagaosa, A. V. Balatsky, Spin current and magnetoelectric effect in noncollinear magnets. *Phys. Rev. Lett.* **95**, 057205 (2005).
16. M. Mostovoy, Ferroelectricity in spiral magnets. *Phys. Rev. Lett.* **96**, 067601 (2006).
17. T. Kimura, Y. Sekio, H. Nakamura, T. Siegrist, A. P. Ramirez, Cupric oxide as an induced-multiferroic with high-T_C. *Nat. Mater.* **7**, 291–294 (2008).
18. Y. Tokura, S. Seki, N. Nagaosa, Multiferroics of spin origin. *Rep. Prog. Phys.* **77**, 076501 (2014).
19. T. Kimura, Magnetoelectric hexaferrites. *Annu. Rev. Condens. Matter Phys.* **3**, 93–110 (2012).

20. M. Fiebig, T. Lottermoser, D. Meier, M. Trassin, The evolution of multiferroics. *Nat. Rev. Mater.* **1**, 16046 (2016).
21. M. Morin, E. Canévet, A. Raynaud, M. Bartkowiak, D. Sheptyakov, V. Ban, M. Kenzelmann, E. Pomjakushina, K. Conder, M. Medarde, Tuning magnetic spirals beyond room temperature with chemical disorder. *Nat. Commun.* **7**, 13758 (2016).
22. L. Er-Rakho, C. Michel, Ph. Lacorre, B. Raveau, $YBaCuFeO_{5+\delta}$: A novel oxygen-deficient perovskite with a layer structure. *J. Solid State Chem.* **73**, 531–535 (1988).
23. Y. K. Atanassova, V. N. Popov, G. G. Bogachev, M. N. Iliev, C. Mitros, V. Psycharis, M. Pissas, Raman- and infrared-active phonons in $YBaCuFeO_5$: Experiment and lattice dynamics. *Phys. Rev. B* **47**, 15201–15207 (1993).
24. M. Morin, A. Scaramucci, M. Bartkowiak, E. Pomjakushina, G. Deng, D. Sheptyakov, L. Keller, J. Rodriguez-Carvajal, N. A. Spaldin, M. Kenzelmann, K. Conder, M. Medarde, Incommensurate magnetic structure, Fe/Cu chemical disorder, and magnetic interactions in the high-temperature multiferroic $YBaCuFeO_5$, *Phys. Rev. B* **91**, 064408 (2015).
25. R. D. Shannon, Revised effective ionic radii and systematic studies of interatomic distances in halides and chalcogenides. *Acta Crystallogr. A* **32**, 751 (1976).
26. D. Dey, S. Nandy, T. Maitra, C. S. Yadav, A. Taraphder, Nature of spiral state and absence of electric polarisation in Sr-doped $YBaCuFeO_5$ revealed by first-principle study. *Sci. Rep.* **8**, 2404 (2018).
27. A. W. Mombru, C. Christides, A. Lappas, K. Prassides, M. Pissas, C. Mitros, D. Niarchos, Magnetic structure of the oxygen-deficient perovskite $YBaCuFeO_{5+\delta}$. *Inorg. Chem.* **33**, 1255–1258 (1994).
28. V. Caignaert, I. Mirebeau, F. Bourée, N. Nguyen, A. Ducouret, J.-M. Greneche, B. Raveau, Crystal and magnetic structure of $YBaCuFeO_5$. *J. Solid State Chem.* **114**, 24–35 (1995).
29. Y.-C. Lai, C.-H. Du, C.-H. Lai, Y.-H. Liang, C.-W. Wang, K. C. Rule, H.-C. Wu, H.-D. Yang, W.-T. Chen, G. J. Shu, Magnetic ordering and dielectric relaxation in the double perovskite $YBaCuFeO_5$. *J. Phys. Condens. Matter* **29**, 145801 (2017).
30. M. J. Ruiz-Aragón, E. Morán, U. Amador, J. L. Martínez, N. H. Andersen, H. Ehrenberg, Low-temperature magnetic structure of $YBaCuFeO_5$ and the effect of partial substitution of yttrium by calcium. *Phys. Rev. B* **58**, 6291–6297 (1998).
31. A. W. Mombrú, K. Prassides, C. Christides, R. Erwin, M. Pissas, C. Mitros, D. Niarchos, Neutron powder diffraction study (T = 4.2–300 K) and polarization analysis of $YBaCuFeO_{5+\delta}$. *J. Phys. Condens. Matter* **10**, 1247–1258 (1998).
32. A. Scaramucci, H. Shinaoka, M. V. Mostovoy, M. Müller, C. Mudry, M. Troyer, N. A. Spaldin, Multiferroic magnetic spirals induced by random magnetic exchanges. *Phys. Rev. X* **8**, 011005 (2018).
33. A. Scaramucci, H. Shinaoka, M. V. Mostovoy, M. Müller, C. Mudry, Spiral order from orientationally correlated random bonds in classical XY models. arXiv: 1610.00784 (2016).
34. R. M. Hornreich, M. Luban, S. Shtrikman, Critical behavior at onset of $\vec{k}$-space instability on the λ–line. *Phys. Rev. Lett.* **35**, 1678–1681 (1975).
35. Y. Shapira, The evidence for a Lifshitz point in MnP (invited). *J. Appl. Phys.* **53**, 1914–1919 (1982).
36. T. Mazet, H. Ihou-Mouko, J.-F. Marêché, B. Malaman, Short-range magnetic order, irreversibility and giant magnetoresistance near the triple points in the (x, T) magnetic phase diagram of $ZrMn_6Sn_{6-x}Ga_x$. *Eur. Phys. J. B.* **74**, 487–497 (2010).
37. R. M. Hornreich, M. Luban, S. Shtrikman, Critical exponents at a Lifshitz point to O(1/*n*). *Phys. Lett. A* **55**, 269–270 (1975).
38. M. Medarde, J. Mesot, P. Lacorre, S. Rosenkranz, P. Fischer, K. Gobrecht, High-pressure neutron-diffraction study of the metallization process in $PrNiO_3$. *Phys. Rev. B* **52**, 9248–9258 (1995).
39. M. Medarde, J. Mesot, S. Rosenkranz, P. Lacorre, W. Marshall, S. Klotz, J. S. Loveday, G. Hamel, S. Hull, P. Radaelli, Pressure-induced orthorhombic- rhombohedral phase transition in $NdNiO_3$. *Physica B Condens. Matter* **234**, 15–17 (1997).
40. J. Sesé, J. Bartolomé, C. Rillo, Disposable sample holder for high temperature measurements in MPMS superconducting quantum interference device magnetometers. *Rev. Sci. Instrum.* **78**, 046101 (2007).
41. S. Lal, K. Mukherjee, C. S. Yadav, Effect of crystalline electric field on heat capacity of $LnBaCuFeO_5$ (Ln = Gd, Ho, Yb). *Solid State Commun.* **270**, 130–134 (2018).
42. A. I. Klyndyuk, Thermoelectric properties of layered ferrocuprates $LnBaCuFeO_{5+\delta}$ (*Ln* = La, Pr, Nd, Sm, Gd-Lu). *Phys. Solid State* **51**, 250 (2009).
43. A. I. Klyndyuk, E. A. Chizhova, Structure and electrical and transport properties of cation-deficient samples of perovskite ferrocuprates $RBaCuFeO_{5+\delta}$ (*R* = Y, La). *Phys. Solid State* **50**, 603 (2008).
44. Y. Kawamura, T. Kai, E. Satomi, Y. Yasui, Y. Kobayashi, M. Sato, K. Kakurai, High-temperature multiferroic state of $RBaCuFeO_5$ (R = Y, Lu, and Tm). *J. Phys. Soc. Jpn.* **79**, 073705 (2010).
45. A. W. Mombrú, A. E. Goeta, H. Pardo, P. N. Lisboa-Filho, L. Suescun, R. A. Mariezcurrena, O. N. Ventura, R. Behak, K. H. Andersen, F. M. Araújo-Moreira, Low-temperature magnetic properties of $LuBaCuFeO_{5+\delta}$ and $TmBaCuFeO_{5+\delta}$. *J. Solid State Chem.* **166**, 251–258 (2002).
46. M. Kochi, J. Lindén, T. Taniyama, K. Lehmus, M. Karppinen, H. Yamauchi, Magnetic properties, oxygen content and metal valences in $BaRE(Cu_{0.5}Fe_{0.5})_2O_{5+\delta}$ with RE=Lu, Yb, Y, Eu, Sm, Nd and Pr. *Physica C Supercond.* **338**, 132–136 (2000).
47. J. Lindén, M. Kochi, K. Lehmus, T. Pietari, M. Karppinen, H. Yamauchi, Interplay between Cu and Fe valences in $BaR(Cu_{0.5}Fe_{0.5})O_{5+\delta}$ double perovskites with *R* = Lu, Yb, Y, Eu, Sm, Nd, and Pr. *J. Solid State Chem.* **168**, 354 (2002).
48. M. Pissas, G. Kallias, A. Simopoulos, D. Niarchos, E. Devlin, R. Sonntag, Mössbauer spectroscopy and neutron diffraction studies of the compound $YSrCuFeO_{5+y}$. *J. Phys. Condens. Matter* **10**, 10317 (1998).
49. S. Lal, S. K. Upadhyay, K. Mukherjee, C. S. Yadav, Evolution of magnetic and dielectric properties in Sr-substituted high-temperature multiferroic $YBaCuFeO_5$. *EPL* **117**, 67066 (2017).
50. J. Rodríguez-Carvajal, Recent advances in magnetic-structure determination by neutron powder diffraction. *Physica B Condens. Matter* **192**, 55–69 (1993).

Acknowledgments: We thank A. Scaramucci, M. Müller, Ch. Mudry, N. Spaldin, M. Shi, Z. Wang, M. Radovic, J. Mesot, R. Sibille, and T. Mazet for fruitful discussions. We acknowledge the allocation of beam time at SINQ (HRPT and DMC diffractometers) and ILL (D2B diffractometer; https://search.datacite.org/data-centers/inist.ill?registered=2018&page=1). E.C. acknowledges support from the Danish Research Council for Science and Nature through DANSCATT. **Funding:** This work was supported by the Swiss National Science Foundation (grant nos. 200021_141334 and 206021_139082). **Author contributions:** T.S. and M.Me. conceived and led the project. T.S., M.Mo., and E.P. synthesized the samples. T.S., E.C., M.Me., D.S., and M.T.F.-D. performed the PND measurements. T.S. measured the magnetic susceptibility and DSC. T.S. and M.Me. analyzed all the experimental data. T.S. and M.Me. wrote the paper with input from all authors. **Competing interests:** The authors declare that they have no competing interests. **Data and materials availability:** All data needed to evaluate the conclusions in the paper are present in the paper and/or the Supplementary Materials. Additional data related to this paper may be requested from the authors. Raw powder diffraction data were generated at the SINQ (Paul Scherrer Institut, Switzerland) and ILL (Grenoble, France). Derived data supporting the results of this study are available from the corresponding authors. FullProf Suite is available free of charge at www.ill.eu/sites/fullprof.

Submitted 1 July 2018
Accepted 19 September 2018
Published 26 October 2018
10.1126/sciadv.aau6386

Citation: T. Shang, E. Canévet, M. Morin, D. Sheptyakov, M. T. Fernández-Díaz, E. Pomjakushina, M. Medarde, Design of magnetic spirals in layered perovskites: Extending the stability range far beyond room temperature. *Sci. Adv.* **4**, eaau6386 (2018).

Design of magnetic spirals in layered perovskites: Extending the stability range far beyond room temperature

Tian Shang, Emmanuel Canévet, Mickaël Morin, Denis Sheptyakov, María Teresa Fernández-Díaz, Ekaterina Pomjakushina and Marisa Medarde

Sci Adv **4** (10), eaau6386.
DOI: 10.1126/sciadv.aau6386